J. CHEM. SOC. FARADAY TRANS., 1991, 87(3), 425–430

Stress-transfer Mechanisms in Electrorheological Suspensions

Daniel J. Klingenberg, Diane Dierking and Charles F. Zukoski
Department of Chemical Engineering, University of Illinois, Urbana IL 61801, USA

The stress transferred by many non-aqueous suspensions can be altered reversibly by the application of large (*ca.* 1 kV mm^{-1}) electric fields. In the presence of an electric field, the suspension at rest is observed to rearrange to a state where the particles form fibres or columns that span the electrode gap. Application of a shear stress to the suspension degrades these structures and the added work required to overcome the electrically induced particle interactions is observed as an increase in the apparent viscosity. In this paper, the origin of the electrorheological response is reviewed and results indicate that, at intermediate shear rates and field strengths, the electrically induced structural alterations give rise to a direct contribution to the apparent viscosity and an indirect contribution, resulting from viscous interactions between particles in the altered structure. At low shear rates, the indirect contribution to the shear stress decreases with decreasing shear rate, while at high shear rates, the shear field is capable of destroying the electrically induced structures and the indirect contribution is again negligible.

Observed in many non-aqueous suspensions, the electrorheological (ER) response is associated with the reversible increase in suspension viscosity upon application of an external electric field. Though first discussed by Winslow in the 1940s,[1] and later by Klass and Martinek in the 1960s,[2,3] application of the ER response to couple mechanical devices in electronic feedback control schemes is currently inhibited by the lack of detailed understanding of stress-transfer mechanisms. In the past decade, renewed interest can be traced to the development of ER fluids based on hydrated polymer particulates which demonstrated potential in a wide range of applications.[4] Over the past five years, the physical principles underlying the ER response have been broadly outlined. However, key features are poorly understood and still subject to debate.[5] This lack of understanding limits the development of useful applications of the ER response.

Recent experimental work has shown that the basic forces underlying the ER response are electrical, viscous, and thermal.[6–8] Electrical forces arise from a dielectric mismatch between the disperse and continuous phases. In the presence of the electric field, the particles polarize and interact through long-range dipolar-like forces, which act to form columns or fibres of particles that span the electrode gap in quiescent suspensions. To understand how polarization forces can give rise to these structures, consider a pair of particles (spheres) of radius a. In a uniform electric field of magnitude E, the force on a particle i at the origin due to another particle j at (R_{ij}, θ_{ij}) is written

$$\boldsymbol{F}_{ij}(R_{ij}, \theta_{ij}) = F_0\left\{\left(\frac{a}{R_{ij}}\right)^4 \times [(2f_{\parallel}\cos^2\theta_{ij} - f_{\perp}\sin^2\theta_{ij})\boldsymbol{e}_r + f_{\Gamma}\sin 2\theta_{ij}\boldsymbol{e}_{\theta}]\right\} \quad (1)$$

$$F_0 = 12\pi\varepsilon_0\varepsilon_c a^2\beta^2E^2$$

where R_{ij} is the distance between particle centres and θ_{ij} is the angle between the line-of-centres and the electric field. Eqn. (1) results from the solution of Laplace's equation for the electrostatic potential around two dielectric spheres in a dielectric continuous phase, subjected to a uniform external electric field.[9] ε_0 is the permittivity of free space and ε_c is the relative permittivity of the continuous phase. $\boldsymbol{e}_r$ and $\boldsymbol{e}_\theta$ are unit vectors pointing parallel and perpendicular to the line-of-centres, respectively. The term $\beta = (\varepsilon_p - \varepsilon_c)/(\varepsilon_p + 2\varepsilon_c)$ is the scaled relative permittivity difference between the continuous and the disperse phases, where ε_p is the disperse-phase relative permittivity. For pairs where $\theta_{ij} = 0$, the polarization force is attractive, while for $\theta_{ij} = \pi/2$, the force is repulsive. At all other angles, the pair experiences a torque tending to align the line-of-centres with the electric field. Thus the electrostatic polarization interaction between particle pairs provides the necessary angular dependence to give rise to particulate columns observed in ER suspensions. The f_i are dimensionless force coefficients that depend on R_{ij}/a and $\varepsilon_p/\varepsilon_c$. In the point-dipole limit, valid for widely spaced particles and/or small β, the f_i are unity.

Marshall *et al.*[6] performed a scaling analysis to show that for a variety of ER suspensions, transport properties can be understood in terms of viscous forces scaling as $6\pi\eta_c a^2\dot{\gamma}$, and polarization forces with a natural scale drawn from eqn. (1) of $12\pi\varepsilon_0\varepsilon_c a^2\beta^2E^2$. Here, η_c is the viscosity of the continuous phase and $\dot{\gamma}$ is the shear rate. (For smaller particles ($a < 1$ μm), thermal forces are significant, but for many ER suspensions which contain large particles and are subjected to large electric fields such that $\varepsilon_0\varepsilon_c a^3\beta^2E^2/k_BT \gg 1$, thermal forces can be neglected.)[7] As a result, Marshall *et al.* were able to combine into a single curve all the viscosity, field strength and shear rate data at a given volume fraction by expressing the dimensionless viscosity η/η_∞ in terms of the Mason number, $Mn = \eta_c\dot{\gamma}/2\varepsilon_0\varepsilon_c(\beta E)^2$. Here η_∞ is the high-shear-rate viscosity of the unelectrified suspension. This analysis suggests that for small values of Mn (large E or small $\dot{\gamma}$), polarization forces dominate the ER response, but at large Mn (small E or large $\dot{\gamma}$) viscous forces control the suspension structure, and thus the mechanism of stress transfer. For all volume fractions studied by these authors, and for a series of separate suspensions,[8] the dimensionless viscosity can be mapped onto a single function of Mn. At small Mn, the $\log(\eta/\eta_\infty) - \log Mn$ curve has a slope of -1, while at large Mn, η/η_∞ smoothly approaches unity. Marshall *et al.* were able to correlate all their data with the Bingham constitutive equation (written in terms of the apparent suspension viscosity)

$$\frac{\eta}{\eta_\infty} = \frac{Mn^*}{Mn} + 1 \quad (2)$$

where Mn^* is a dimensionless yield stress that is independent of field strength and shear rate but depends on the volume fraction and the material properties of the disperse and continuous phases. Mn^*, typically $\mathcal{O}(1)$, represents the characteristic value of Mn where the transition between electrostatically and hydrodynamically controlled stress

transfer occurs. Later work has shown that the same scaling holds for suspensions of polyaniline particles doped to different values of ε_p.[8] In these experiments, Mn^* increased monotonically with β.

The Bingham model is found to provide an excellent correlation for viscosity–shear rate data at low and high values of Mn but to underpredict the stress transferred in ER suspensions at Mn^*/Mn of order unity. Recently, the poor predictive capability of the Bingham model has been attributed to the non-uniform degradation of the polarization induced structures at intermediate shear rates.[9] This work has led to interest in the relative importance of polarization and shear forces. Three detailed modelling efforts have addressed these questions.

Adriani and Gast[10] have developed a model for ER suspensions applicable in the limit of small, Brownian particles and low electric field strengths [$\varepsilon_0 \varepsilon_c a^3 \beta^2 E^2 / k_B T = \mathcal{O}(1)$]. This model captures the electric field strength scaling observed in ER suspensions but fails to predict the experimentally observed static yield stress. Recently, several computer simulation studies of ER suspensions have been initiated.[11–13] Addressing the small-Mn limit, a simulation of suspension structure formation and degradation has been developed.[11] In this model, the particles interact as point-dipoles with hard core repulsions, and experience Stokes' drag, neglecting interparticle hydrodynamic interactions. Results of two- and three-dimensional simulations confirm the dominance of the angular dependence of the electrostatic polarization interaction [eqn. (1)] in determining quiescent suspension structure. More recent simulations of the shear stress developed in ER suspensions at small shear rates indicate that this model also captures the observed volume fraction dependence of the yield stress.[14] Bonnecaze and Brady[12] have conducted a study of ER suspension flow with a Stokesian dynamics simulation which accounts for multibody hydrodynamic and electrostatic interactions. Owing to computational complexity, these simulations are currently limited to a monolayer of particles at intermediate area fractions. However, the results indicate that at intermediate Mn (i.e. Mn^*/Mn of order unity), viscous interactions are as significant as polarization interactions.

While the ER response is dominated by the interparticle polarization forces in the small-Mn limit, these modelling studies suggest that hydrodynamic forces have significant impact on the stress transfer at intermediate Mn. For instance, as the electrostatic forces hold particles close together, lubrication forces may be expected to contribute at finite strain rates. Also, since the electrostatic interaction between particles is strongly dependent upon pair orientation, any alteration in the suspension structure due to hydrodynamic forces will affect the electrostatic contribution to stress transfer. We present experiments aimed at evaluating the relative importance of hydrodynamic forces and polarization forces in the stress-transfer properties of ER suspensions.

Experimental

The ER suspensions studied here are composed of 20 wt.% hollow silica spheres (P. A. Industries) with an average particle diameter of 60 μm. The particles have an average apparent density of 0.74 g cm^{-3}, and a relative permittivity $\varepsilon_p = 11$, and are suspended in corn oil (0.055 Pa s, 0.92 g cm^{-3}, $\varepsilon_c = 2.9$). All measurements were performed with a 3 kV DC power supply. The current passed through the suspension was continuously monitored during the experiments, and the current density was always less than 0.2 A m^{-2}.

Rheological properties of this suspension were determined using a modified Bohlin (Lund Sweden) rheometer with a cup and bob geometry. The cup was driven at a known angular velocity, and the stress transferred to the bob was measured *via* a torque transducer. The cup was composed of Delrin with a stainless-steel inner sleeve, electrical contact being achieved through a sliding electrode. The inner diameter of the cup was 15.2 mm while the stainless-steel bob, 21.5 mm in height, had an outer diameter of 14.0 mm, providing a gap of 0.6 mm. The bob was attached to the torque transducer through a Delrin insulating coupling. Electrical contact to the bob was achieved through a light, insulated transformer wire connected with a set screw. All experiments were carried out at 25 °C.

Two types of experiments were used to characterize the stress-transfer mechanisms in this ER suspension. Primarily, the shear stress was measured as a function of shear rate under steady-state conditions. The shear stress measured was found to be reproducible provided sufficient equilibration time was allowed following a change in the applied shear rate. The required equilibration time depends on the shear history, but the value of the stress at steady state does not. In the experiments reported here, the desired electric field was applied to the static suspension for 5 min. At this point, the highest shear rate desired was applied to the suspension and maintained for an equilibration time of 500 s. The stress was then measured continuously over the next 100 s and the average value recorded. The next lower desired shear rate was then applied and the process repeated (500 s equilibration time, 100 s measurement time). Following this procedure, the measured stresses were reproducible and insensitive to increases in the equilibration and measurement times.

Secondly, flow-relaxation experiments were used to determine the extent to which the stress transferred was of viscous origin. Here, the suspension was sheared at a fixed shear rate with the electric field applied until steady state was achieved. The shear rate was then set to zero and the time evolution of the shear stress measured.

Flow-visualization experiments were performed to investigate structural changes during shear in ER suspensions. The experimental method has been described elsewhere;[9] only a brief outline will be presented here. The suspension was placed between two parallel plate brass electrodes. The bottom electrode, 0.4 cm × 5.7 cm × 187 cm, was held within a Plexiglass trough. The top electrode, 0.4 cm × 5.0 cm × 91 cm was held 2.0 mm above the bottom electrode on an insulating Plexiglass fixture. The fixture was mounted on a rail and connected to a pan motor allowing it to be driven at velocities in the range 1 mm s^{-1}–5 cm s^{-1}. A video camera was focused on the suspension and the image recorded on videotape. In all experiments reported here, the applied field strength was 750 V mm^{-1}.

Results and Discussion

Upon application of an electric field to the suspension of silica spheres, the particles rearrange into columns or fibres that span the electrode gap, Fig. 1. This type of structural rearrangement was reported by Winslow in his original description of the ER response[1] and has been reported many times subsequently. Under small shear strains (slight displacement of the top electrode), the columns deform in an elastic manner. At small, steady shear rates, the fibres are observed to continually break and reform, and show a tendency to form somewhat larger, dense clusters. The elastic response of the structures subjected to small strains or stresses[8] suggests that the columns display solid-like mechanical properties. Spanning the electrode gap at small shear rates, with increas-

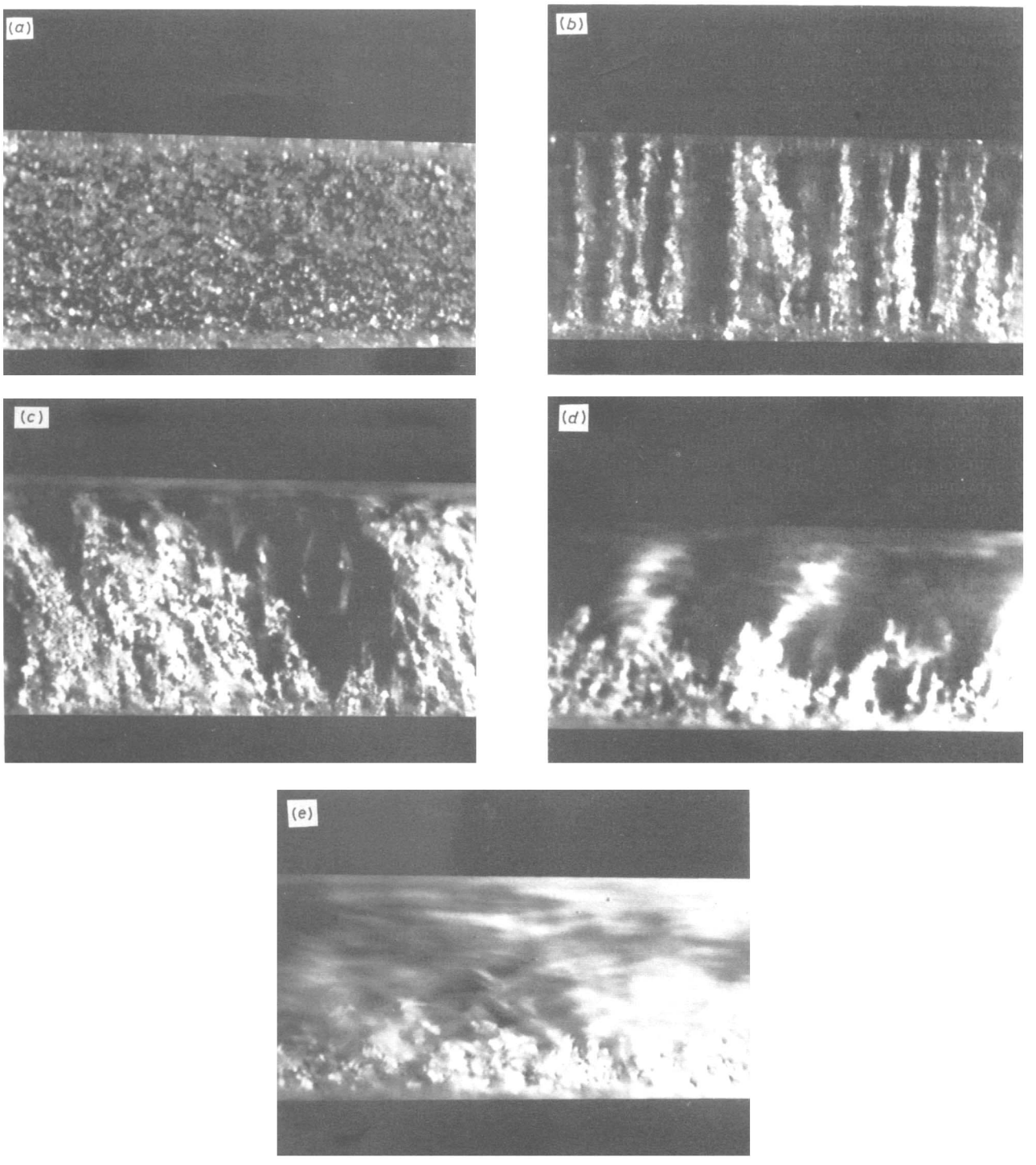

Fig. 1 Photographs of an ER suspension (*a*) $E = 0$ V mm^{-1}, $\dot{\gamma} = 0$ s^{-1}; (*b*) $E = 750$ V mm^{-1} $\dot{\gamma} = 0$ s^{-1}; (*c*) $E = 750$ V mm^{-1}, $\dot{\gamma} = 0.5$ s^{-1}, $Mn = 4 \times 10^{-3}$ (the top electrode is moving to the left); (*d*) $E = 750$ V mm^{-1} $\dot{\gamma} = 3$ s^{-1}, $Mn = 2 \times 10^{-2}$ (the top electrode is moving to the right); (*e*) $E = 750$ V mm^{-1}, $\dot{\gamma} = 10$ s^{-1}, $Mn = 8 \times 10^{-2}$ (the top electrode is moving to the left)

ing rates of deformation, the solid-like structures are observed to be degraded in a sequential manner. As the shear rate is increased, a region is formed near the centre of the gap, parallel to the electrode surfaces, containing fewer particles than the suspension on average. Owing to the lack of gap-spanning fibres, this region is referred to as fluid-like. Particles in this zone appear as streaks in the videotape frame. Next to the fluid-like region are solid-like regions that are attached to the electrodes and static (with respect to the electrode surface). As the shear rate is further increased, the fluid-like gap expands, with the field-induced structures completely degraded at the highest shear rates.

A lack of particulate strands percolating in the direction of the electric field distinguishes the fluid-like zones from solid-like zones. As a result, while clusters of particles are observed in the fluid-like zone, the primary means of stress transfer in this region will be viscous. If the shear rate is set to zero, the stress should relax to zero at a rate commensurate with that of a viscous suspension. Alternatively, the solid-like regions contain columns or large clusters of particles that remain attached to the electrodes. When these structures span the electrode gap, the primary means of stress transfer will be electromechanical and, if the shear rate is set to zero, the stress should relax due to structural rearrangement at a much

slower rate than that of a viscous suspension. The suspension pictured in Fig. 1 has a volume fraction of 0.02, substantially lower than that used in typical electrorheological suspensions. Observation of concentrated suspensions confirms the qualitative features pictured, suggesting that the polarization induced structures are expected to be of primary significance in determining stress transfer at low shear rates.

The shear stress of the model ER suspension is plotted against shear rate at several electric field strengths, Fig. 2. As the shear rate decreases, the measured shear stress reaches a plateau. The shear rate at which the plateau begins and the magnitude of the plateau stress depend on the magnitude of the electric field strength. Since the value of the plateau stress is the value obtained by extrapolating the data to zero shear rate, this plateau stress represents a dynamic yield stress.

At these small shear rates (small Mn), the stress is independent of shear rate, *i.e.* decreasing the shear rate by, say, a factor of 10 has no effect on the shear stress. The lack of dependence of the shear stress on the shear rate, and the dependence of the plateau stress (dynamic yield stress) on E^2 indicates that in this small shear rate regime ($Mn \ll 1$), the stress transfer is purely electrostatic. Thus, we may write

$$\tau = \tau_y(E); \quad Mn/Mn^* \ll 1$$

where τ_y is the dynamic yield stress. The electrostatic scaling used in the development of the Mason number indicates that τ_y increases with the square of the electric field strength. Mn^* is found to be 0.5 by performing a least-squares fit of the data in Fig. 3 (where the relative suspension viscosity is plotted against the Mason number for several electric field strengths) to eqn. (2).

At very large shear rates (large Mn), the suspension viscosity becomes that of the unelectrified suspension. Under these conditions, viscous forces are much larger than polarization forces and the fibrous structures are entirely degraded. As a result, varying the electric field strength has no effect on the suspension viscosity, and the stress is thus transferred by purely viscous means. In this limit we may write

$$\tau = \eta_\infty \dot{\gamma}; \quad Mn/Mn^* \gg 1$$

where, again, η_∞ is the high shear rate viscosity of the unelectrified suspension.

At intermediate shear rates [$Mn^*/Mn = \mathcal{O}(1)$], however,

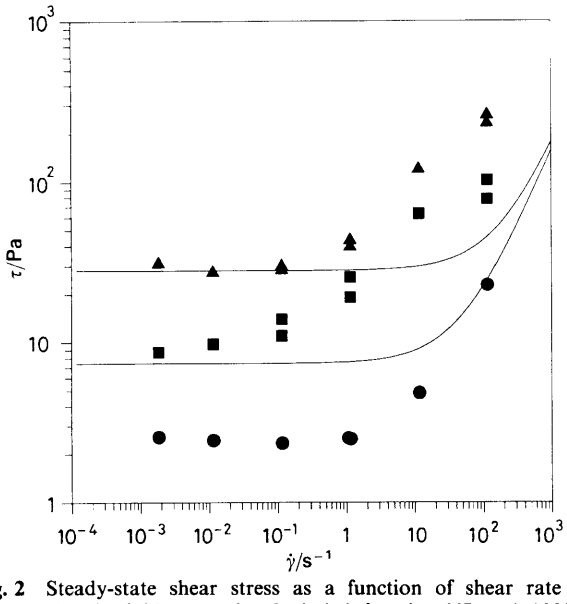

Fig. 2 Steady-state shear stress as a function of shear rate for several electric field strengths. Included for the 667 and 1333 V mm^{-1} results are the Bingham relationships [solid lines, see eqn. (2)] derived from the small and large shear rate limits of the data. ●, 0 V mm^{-1}; ■, 667 V mm^{-1}; ▲, 1333 V mm^{-1}

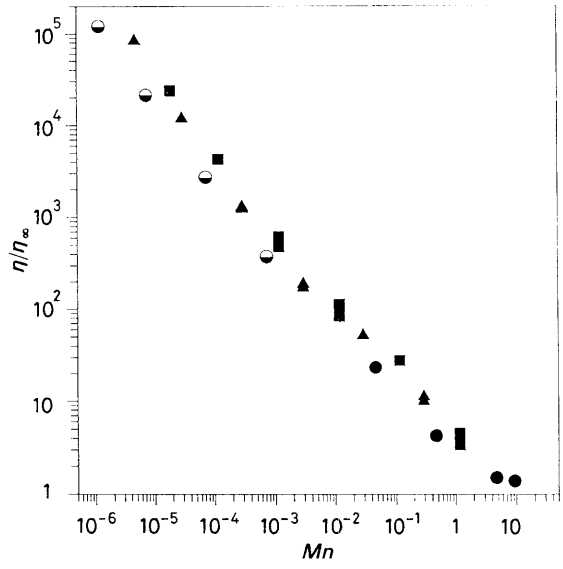

Fig. 3 Relative suspension viscosity as a function of Mason number at several electric field strengths. The relative suspension viscosity is defined as the apparent suspension viscosity divided by the high-shear-rate viscosity of the unelectrified suspension. ●, 333 V mm^{-1}; ■, 667 V mm^{-1}; ▲, 1333 V mm^{-1}; ◒, 2667 V mm^{-1}

hydrodynamic and electrostatic polarization contributions to the shear stress are of comparable magnitudes. Indeed, one might expect a synergistic interaction between hydrodynamic and electromechanical stress transfer due to the indirect influence one mode will have on the other through alterations in the suspension structure. For instance, in the small-shear-rate regime, stress is transferred purely in an electromechanical fashion through the percolating chains. With increasing shear rate, hydrodynamic forces begin to influence the structure of the percolating chains and therefore indirectly influence the electromechanical stress transfer. Similarly, in the large-shear-rate regime, the stress transfer is purely viscous and the suspension structure is independent of electric field strength. However, with a reduction in the shear rate or an increase in the electric field strength, polarization forces begin to influence the suspension structure. Small strand-like aggregates form and dielectrophoresis creates solid-like regions at the electrode walls with the fluid-like region in between. Both the presence of clusters and the effectively reduced gap increase the apparent viscosity (through increased energy dissipation). As a result, the electrostatic forces indirectly influence the viscous stress transfer through changes in the suspension structure.

While the magnitude of the synergistic stress can be estimated from simulations, measuring its magnitude presents a difficulty. We have chosen to express a measure of this stress in terms of a modified Bingham constitutive equation.

$$\tau(\dot{\gamma}, E) = \tau_y(E) + \eta_\infty \dot{\gamma} + \tau_{ex}(\dot{\gamma}, E) \qquad (3)$$

$\tau_y(E)$ is the dynamic yield stress, $\eta_\infty \dot{\gamma}$ is the viscous contribution to the shear stress at large shear rates and no electric field, and $\tau_{ex}(\dot{\gamma}, E)$ is the excess stress representing the coupling of hydrodynamic and electrostatic polarization interactions described above. We note here that this definition of the cross term, $\tau_{ex}(\dot{\gamma}, E)$, is made somewhat arbitrarily, and is simply the stress above and beyond the sum of the two 'pure' limits. However, $\tau_{ex}(\dot{\gamma}, E)$ represents a rough measure of the cross term and is defined in terms of experimentally determined quantities. If the structure is determined by the Mason number, then $\tau_{ex}(\dot{\gamma}, E)$ should also depend only on this quantity. As shown in Fig. 4, where $\tau_{ex}(Mn)$ is given as a fraction of $\tau_y(E) + \eta_\infty \dot{\gamma}$, this expectation is apparently met.

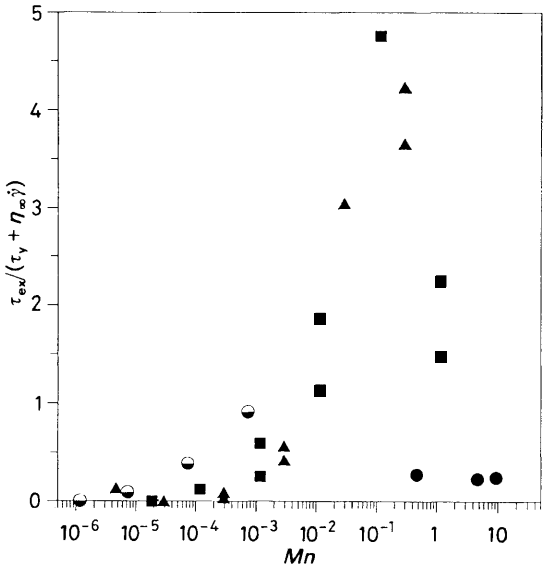

Fig. 4 Reduced excess stress [see eqn. (3)] as a function of Mason number at several electric field strengths. The average uncertainty in the reduced excess stress is *ca.* 10%. ●, 333 V mm^{-1}; ■, 667 V mm^{-1}; ▲, 1333 V mm^{-1}; ◒, 2667 V mm^{-1}

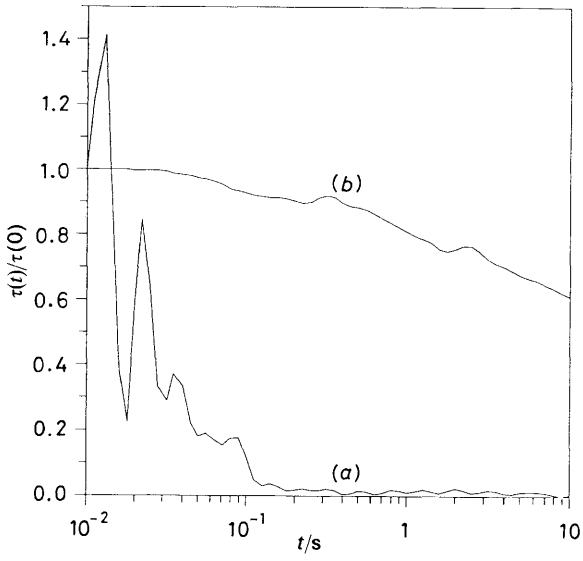

Fig. 5 Stress relaxation in the small- and large-shear-rate regimes. The stress as a function of time has been normalized by the stress at $t = 0$. (*a*) 0 V mm^{-1}, 116 s^{-1}; (*b*) 1333 V mm^{-1}, 0.0116 s^{-1}

At small shear rates or large electric field strengths, the excess stress approaches zero as expected, while in the limit of large shear rates, $\eta_\infty \dot{\gamma}$ dominates eqn. (3), and again, $\tau_{ex}(Mn)/[\tau_y(E) + \eta_\infty \dot{\gamma}]$ decreases. At intermediate *Mn*, the synergistic effect between polarization forces and viscous forces becomes apparent and $\tau_{ex}(Mn)/[\tau_y(E) + \eta_\infty \dot{\gamma}]$ passes through a maximum. The maximum is observed at an *Mn* of order unity (*ca.* 0.1) indicating that synergistic effects are largest when hydrodynamic and polarization forces are of the same order of magnitude. Surprisingly, the excess stress at the maximum is 4–5 times larger than $\tau_y(E) + \eta_\infty \dot{\gamma}$. Determination of $\tau_{ex}(Mn)/[\tau_y(E) + \eta_\infty \dot{\gamma}]$ for other systems[6,14] indicates that the maximum value of $\tau_{ex}(Mn)/[\tau_y(E) + \eta_\infty \dot{\gamma}]$ is an $\mathcal{O}(1)$ quantity, with the actual value as well as the value of *Mn* at the maximum being system dependent. However, all suspensions investigated show the same qualitative behaviour for $\tau_{ex}(Mn)/[\tau_y(E) + \eta_\infty \dot{\gamma}]$ as shown in Fig. 4, *i.e.* a broad peak roughly centred at *Mn**.

Further evidence of the synergistic effects of combined shear and electric fields on stress transfer in ER suspensions comes from flow-relaxation studies. When polarization induced structures are degraded by shear, Fig. 1, a fluid-like zone develops where the primary means of stress transfer becomes viscous in nature, and, upon cessation of flow, the shear stress should relax at a rate characteristic of a suspension with no electric field applied. Alternatively, if strain and rupture of fibres is the primary means of stress transfer then, upon cessation of flow, the shear stress should relax on a timescale characterizing rearrangement of these polarization induced structures (*i.e.* a time much longer than for the unelectrified suspension). Typical flow relaxation curves are shown in Fig. 5. As expected, the shear stress in the unelectrified suspension relaxes to half its steady-state value in *ca.* 0.03 s for all shear rates studied. (Owing to low levels of stress transferred in the unelectrified suspension, inertial effects and instrument noise give rise to non-monotonic stress relaxation curves.) As electric field strength is increased, the time required for the stress to relax to half its steady-state value remains *ca.* 1.5–3 times the value for the unelectrified suspension until *Mn* values of the order of 1×10^{-2} are reached (Fig. 6), indicating that for *Mn* greater than this value, fluid-like zones transfer stress in the electrified suspension. For smaller *Mn*, the relaxation time grows substantially, suggesting that rearrangement of gap-spanning structures provides the dominant stress relaxation mechanism. While large relaxation times provide evidence for the presence of fibres spanning the electrode gap for $Mn < 1 \times 10^{-2}$, the observed maximum in $\tau_{ex}(Mn)/[\tau_y(E) + \eta_\infty \dot{\gamma}]$ is observed at $Mn \approx 1 \times 10^{-1}$. Thus while the synergistic effects of hydrodynamic and polarization forces enhance stress transfer while percolating strands are present, the coupling is most apparent just after the fluid-like region forms.

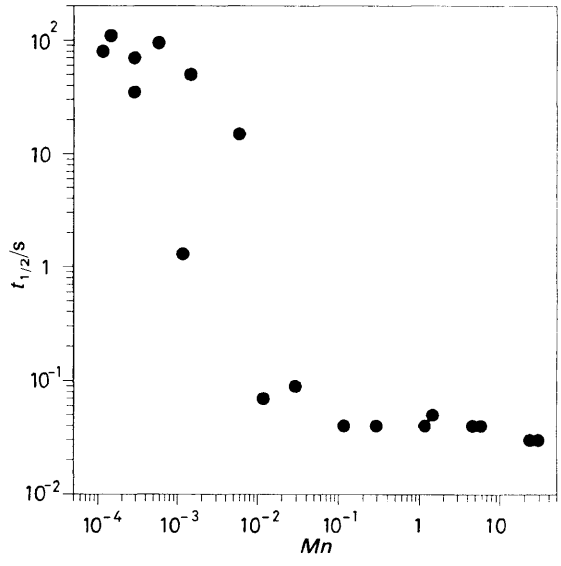

Fig. 6 Characteristic time for stress relaxation as a function of Mason number. The characteristic time is defined as the time required for the stress to relax to half its initial value

Conclusion

The results presented here suggest that for $Mn \ll Mn^*$, stress is transferred between the electrodes by an electromechanical mechanism through percolating particle strands. For the suspension studied, as the shear rate is increased or the electric field strength decreased such that *Mn* approaches a value of

ca. 1×10^{-4}, hydrodynamic forces begin to influence the stress transfer through alterations in the suspension structure, as observed by an increase in $\tau_{ex}(Mn)/[\tau_y(E) + \eta_\infty\dot{\gamma}]$ from zero. At intermediate Mn, both before and after the percolating structures are destroyed by increasing the shear rate, stress transfer is a combination of electrostatic and hydrodynamic mechanisms, with the actual value being greater than that expected by a simple summation of these two mechanisms in their limiting forms. This difference is seen as a cross term, $\tau_{ex}(Mn)$ defined in eqn. (3), arising from indirect contributions of one mechanism to the other through alterations in the suspension structure. This cross term passes through a maximum as Mn increases, and eventually approaches zero. In the large Mn region, hydrodynamic forces dominate over polarization forces and the structure, as well as the shear stress, is determined only by the hydrodynamic forces.

Analysing the exact origin of the excess stress is beyond the scope of the current paper. However, we feel that the excess stress seen in ER suspensions is analogous to the effects of shear on the viscosity of stable, Brownian colloidal suspensions where shear gives rise to a direct contribution to the stress through increases in the local shear rate near particle surfaces and an indirect contribution due to distortions in the suspension structure.[15] At small Mn, suspension structure is controlled by polarization forces. When large enough to distort the polarization induced structure to an appreciable extent, hydrodynamic forces acting on the particles give rise to an indirect contribution to the stress. At still larger shear rates, the structure is dominated by hydrodynamic interactions, and electric field induced interactions alter the suspension structure from that expected when $E = 0$. In the limit of $E \to 0$ or $\dot{\gamma} \to \infty$, the indirect contribution to the stress is negligible. Future work will concentrate on developing an understanding of the origins of the excess stress in these terms and in explaining the large magnitude of the excess stress. We close by noting that the excess stress reaches a value of *ca.* 10 times that of the electrically induced yield stress, a result of some importance to those attempting to choose operating regimes for ER suspensions.

References

1 W. M. Winslow, *J. Appl. Phys.*, 1949, **20**, 1137.
2 D. L. Klass and T. W. Martinek, *J. Appl. Phys.*, 1967 **38**, 67.
3 D. L. Klass and T. W. Martinek, *J. Appl. Phys.*, 1967 **38**, 75.
4 D. Scott, *Pop. Sci.*, April 1984, **82**.
5 R. Pool, *Science*, 1990, **247**, 1180.
6 L. Marshall, C. F. Zukoski, and J. W. Goodwin, *J. Chem. Soc., Faraday Trans. 1*, 1989, **85**, 2785.
7 A. P. Gast and C. F. Zukoski, *Adv. Colloid Interface Sci.*, 1989, **30**, 153.
8 C. J. Gow and C. F. Zukoski, *J. Colloid Interface Sci.*, 1990, **136**, 175.
9 D. J. Klingenberg and C. F. Zukoski, *Langmuir*, 1990, **6**, 15.
10 P. M. Adriani and A. P. Gast, *Phys. Fluids*, 1988, **31**, 2757.
11 D. J. Klingenberg, F. van Swol and C. F. Zukoski, *J. Chem. Phys.*, 1989, **91**, 7888.
12 R. T. Bonnecaze and J. F. Brady, presented at the 2nd International Conference on Electrorheological Fluids, Raleigh, NC, August, 1989.
13 P. Bailey, D. G. Gillies, D. M. Heyes and L. H. Sutcliffe, *Mol. Sim.*, 1989, **4**, 137.
14 D. J. Klingenberg, F. van Swol, and C. F. Zukoski, to be submitted.
15 W. B. Russel and A. P. Gast, *J. Chem. Phys.*, 1986, **84**, 1815.

Paper 0/02311F; *Received* 23*rd May*, 1990.